Mass spectrometry study of the temperature dependence of Pt film growth by atomic layer deposition

ECS Journal of Solid State Science and Technology, **1** (6) P255-P262 (2012)
2162-8769/2012/1(6)/P255/8/$28.00 © The Electrochemical Society

Mass Spectrometry Study of the Temperature Dependence of Pt Film Growth by Atomic Layer Deposition

I. J. M. Erkens,[a,b,z] A. J. M. Mackus,[a] H. C. M. Knoops,[a] P. Smits,[a] T. H. M. van de Ven,[a] F. Roozeboom,[a,*] and W. M. M. Kessels[a,*]

[a]*Eindhoven University of Technology, 5600 MB Eindhoven, The Netherlands*
[b]*Holst Centre (IMEC-NL), 5605 KN Eindhoven, The Netherlands*

Insights into the temperature dependence of atomic layer deposition (ALD) of Pt using (methylcyclopentadienyl)trimethylplatinum, (MeCp)$PtMe_3$, precursor and O_2 are presented, based on a study of reaction products by time-resolved quadrupole mass spectrometry (QMS) measurements. Above 250°C, Pt ALD proceeds through unhindered O_2 dissociation at the Pt surface, inducing complete and instantaneous combustion of the precursor ligands. Quantification of the QMS data revealed that at 300°C, approximately 20% of the C-atoms react during the precursor pulse, forming mainly CH_4 (∼18%) balanced by CO_2 (∼2%). The remaining 80% of the C-atoms are combusted during the O_2 pulse. Time-resolved data indicated that the combustion reactions compete with the hydrogenation reactions for the available surface carbon. Combustion reactions were found to be dominant, provided that a sufficient amount of chemisorbed oxygen is available. When the temperature drops below 250°C, deposition becomes hindered by the presence of a carbonaceous surface layer of partially fragmented and dehydrogenated precursor ligands, formed during the precursor pulse. The carbonaceous layer limits dissociative chemisorption of O_2 and hence combustion reactions (leading to CO_2) whereas reduced surface reactivity also limits (de-)hydrogenation reactions (leading to CH_4). Below 100°C, the carbonaceous layer fully prevents O_2 dissociation and ALD of Pt cannot proceed.
 [DOI: 10.1149/2.006206jss]

Manuscript submitted July 16, 2012; revised manuscript received August 23, 2012. Published September 27, 2012.

Atomic layer deposition (ALD) of Pt-group metals and their oxides on high aspect ratio 3-D nanostructures, can have a wide variety of applications in nanoelectronics as well as in sensing and catalysis.[1–9] One noble metal ALD process that has attracted a lot of recent attention is that of platinum, based on (methylcyclopentadienyl)trimethylplatinum precursor ((MeCp)$PtMe_3$) and O_2 gas, as developed by Aaltonen et al.[10] As it is amongst the most widely applied and studied processes, it can be considered a model system for noble metal ALD processes that are based on the availability of chemisorbed surface oxygen at the start of each precursor pulse. Several studies have been performed on the reaction products that are produced during the process, to obtain information about surface reactions and to better understand the reaction mechanism.[11–14] Extending the work of Aaltonen et al.,[10] Kessels et al.[12] describe a possible reaction mechanism of the process at 300°C:

$$2(\mathrm{MeCp})\mathrm{PtMe_3(g)} + 3\ \mathrm{O(ads)} \rightarrow 2(\mathrm{MeCp})\mathrm{PtMe_2(ads)} + \mathrm{CH_4(g)} + \mathrm{CO_2(g)} + \mathrm{H_2O(g)} \quad [1]$$

$$2(\mathrm{MeCp})\mathrm{PtMe_2(ads)} + 24\ \mathrm{O_2(g)} \rightarrow 2\ \mathrm{Pt(s)} + 3\ \mathrm{O(ads)} + 16\ \mathrm{CO_2(g)} + 13\ \mathrm{H_2O(g)}. \quad [2]$$

This mechanism was based on steady-state gas phase FTIR experiments in a cold-wall reactor at an O_2 pressure of 1 mbar. By balancing the carbon containing volatile reaction products, on average approximately 1 C-atom per precursor molecule was found to be removed during the precursor pulse. This occurs through combustion of the ligands by chemisorbed oxygen producing CO_2 and H_2O, as well as through the production of CH_4, with an observed CH_4 / CO_2 ratio of 1:1. During the subsequent O_2 step, the remaining hydrocarbon ligands, that constitute ∼87% of the precursor carbon, are combusted by O_2 gas. Overall, this reaction mechanism was also confirmed by Christensen et al.[13] who analyzed the process at 300°C in a viscous flow reactor using QMS and quartz crystal microbalance (QCM) techniques. Their study confirmed that the majority of the C-atoms is combusted during the O_2 pulse, although the ratio of CH_4 / CO_2 production during the precursor pulse was found to be 5:1 instead of 1:1.

Despite these and other studies, several questions remain concerning the reaction mechanism of the Pt ALD process. One characteristic of the Pt ALD process that is still not fully understood is the temperature dependence of the growth per cycle (GPC). Knoops et al. showed that the growth of platinum is relatively constant between 300 and 250°C, while the GPC decreases between 250 and 150°C, and growth is inhibited for substrate temperatures of 150°C and lower.[15] This behavior was also confirmed by new experiments (see Figure 1). An explanation for the reduced growth at lower temperatures was not given, although it was inferred from surface science studies that the dissociative chemisorption of O_2 should not be the limiting factor.

Another matter that could benefit from further study is the fact that reaction Equations 1 and 2 are overall reactions, and give no information on individual reaction paths or on the reaction kinetics. Whereas CO_2 and H_2O can be ascribed to combustion by chemisorbed oxygen, some debate remains on the exact nature of the reaction leading to the production of CH_4 and the interdependency between the production of CH_4 and CO_2 / H_2O. Elliott et al. suggest the involvement of in-situ created hydroxyl groups in the formation of CH_4, although to date the presence of OH groups has not been confirmed to the best of our knowledge.[16] Mackus et al. make a strong case for the possibility of hydrogenation of the hydrocarbon surface ligands leading to the production of CH_4.[17]

To gain more insight into both the temperature dependence of the reaction mechanism, and to increase understanding of reaction kinetics, more data and especially time-resolved data is required. In the present work, the issue of both the temperature dependence of the GPC and the reaction kinetics is addressed on the basis of time-resolved QMS measurements carried out in an ALD temperature series. An explanation for the temperature dependence of the GPC and the inhibition of growth at lower temperatures by surface poisoning is given. Furthermore, the insights that were gained into the surface reactions and reaction rates during Pt ALD are described, showing that the reactions leading to the production of CH_4 compete with combustion reactions producing CO_2.

Experimental

Experimental setup.— All measurements were performed in an open load home-built ALD reactor. It consists of a deposition chamber containing a substrate heating stage, connected to an inductively coupled plasma source (100 W) and a turbomolecular pump through gate valves. The temperature of the reactor walls T_w, which can be raised to 150°C, was kept at 80°C (unless mentioned otherwise) to prevent reactions from taking place at the walls, as will be explained later. The temperature of the substrate stage was varied between 80 and 300°C.

*Electrochemical Society Active Member.
[z]E-mail: i.j.m.erkens@tue.nl

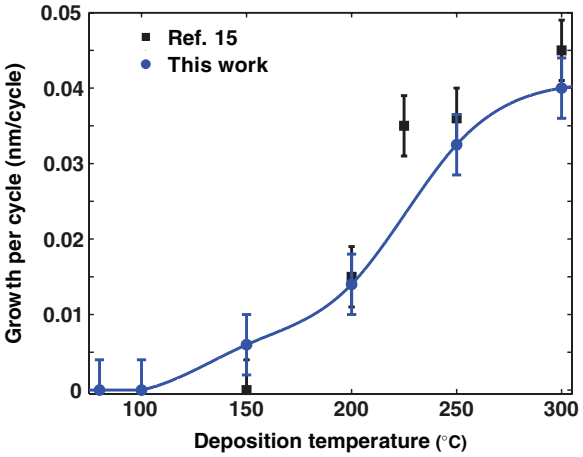

Figure 1. The growth per cycle as a function of deposition temperature (curve serves as a guide to the eye). All depositions were carried out on as-deposited platinum seed layers with a thickness of 13 nm. Data from Knoops et al.[15] are given for comparison.

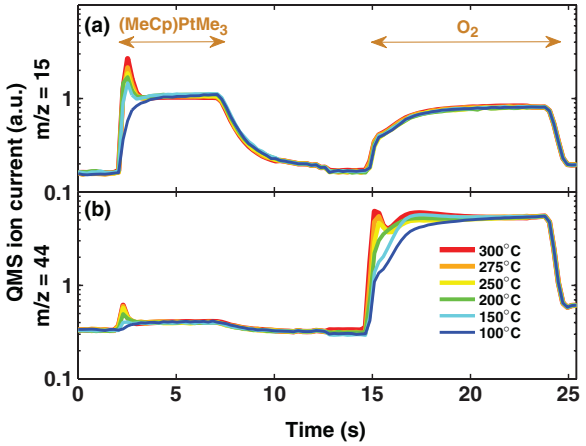

Figure 2. (Color online) Time resolved QMS signal for different substrates temperatures for (a) $m/z = 15$ (CH_3^+ from CH_4 and (MeCp)$PtMe_3$) and (b) $m/z = 44$ (CO_2^+ from CO_2). The precursor pulse (5 s) and O_2 pulse (10 s) are indicated by arrows for clarity. Comparison to *precursor only* and *oxygen only* data showed that at 100°C, virtually no reaction products are produced. The thinnest (blue) line can therefore be regarded as a baseline for the other data.

The (MeCp)$PtMe_3$ precursor (98% purity, Sigma-Aldrich), kept at a temperature of 70°C, was vapor drawn into the reactor without any carrier gas and the precursor dosing time was typically 5 s. The O_2 flow was controlled using a mass flow controller to obtain a 10 s pulse with a stable pressure of 0.08 mbar. During the ALD cycles, the reaction chamber was continuously pumped by the turbomolecular pump. The pressure inside the deposition chamber varied from the base pressure of the order of 10^{-6} mbar during the 30 s pump-down step, to 0.08 mbar during the O_2 pulse.

A Pfeiffer Vacuum QMS 200 mass spectrometer with a mass-to-charge (m/z) range of 200 atomic mass units (amu) was connected to the deposition chamber through a pipeline (kept at 80°C) and a 150 μm pinhole. A channeltron detector was used, and the energy of the electrons in the ionizer was set to 70 eV. In-situ spectroscopic ellipsometry (SE) was performed using a J. A. Woollam, Inc. M2000U ellipsometer to determine the thickness of the deposited layers. For the modeling of the dielectric function of the deposited layers, a Drude-Lorentz parameterization was used, assuming that every film consists of a homogeneous layer of Pt.[15] During standard SE monitoring, every measurement was performed after a complete cycle, immediately giving the GPC. During some experiments however the SE measurements were performed after every half-cycle, i.e. after every precursor step and after every O_2 step.[18] This was done to obtain insight into the effects of precursor absorption and subsequent combustion on the apparent thickness of the film.

QMS measurement procedure.— Performing QMS measurements during an ALD process poses several opportunities and challenges, and special care must be taken when recording and analyzing the data.[19] The measurement procedure that was developed for this work will be described based on the measurements shown in Figure 2. This figure shows the measured QMS ion current as a function of time for substrate temperatures between 100 and 300°C (T_{wall} = 80°C). Precursor and O_2 pulse durations are indicated by arrows for clarity. As in previous studies[12,13] a scan of all relevant m/z ratios revealed that H_2O, CH_4 and CO_2 are the only gas phase reaction products that could be detected using QMS. In particular, measurements of $m/z = 79$ for the methylcyclopentadienyl ligand ($(C_5H_4)CH_3^+$) did not reveal this ligand as a reaction product, although it clearly appeared as a fragment in the precursor cracking pattern. Detection of H_2 as a reaction product proved challenging due to the abundance of $m/z = 1$ and 2 in the cracking pattern of the precursor and other species (e.g. CH_4 and H_2O). Therefore, although it was not detected, the production of H_2 could not be excluded based on the measurements performed here. Furthermore, because the detection of H_2O can be troubled by condensation of water on the colder reactor walls and QMS line, the focus of the QMS analysis was on CH_4 and CO_2. To track CO_2, $m/z = 44$ was recorded, and for CH_4 the fragment at $m/z = 15$ (CH_3^+) was chosen rather than the signal due to the parent molecule at $m/z = 16$, to avoid interference from the signal caused by cracking of O_2. The sensitivity of the QMS for $m/z = 15$ and 44 is assumed to be constant. The QMS data shown in Figure 2 is based on measurements of ALD depositions on as-deposited Pt films under steady-state conditions, free from nucleation or start-up effects. The signals for $m/z = 15$ and 44 were recorded simultaneously to prevent any manual time alignment errors. A dwell-time of 0.05 s ensured that the systematic time alignment error caused by mass filter switching and settling did not exceed 0.1 s. The repetitive nature of ALD was optimally utilized to increase the signal-to-noise ratio (SNR) of the measurements: since every cycle can be assumed to be identical to the next, the QMS data of several cycles was aligned to overlap in time and then averaged, using a dedicated MATLAB algorithm. As a result, every line in Figure 2 represents the average of at least 10 ALD cycles.

The interpretation of the data is not straightforward because of two effects: m/z overlap and a pressure artifact. The former concerns the overlap between signals from reaction products and the precursor. As molecules are ionized through electron bombardment in the ionizer, several of them will break down into smaller fragments. These fragments, which in the case of the precursor form a broad spectrum of m/z ratios including 15 and 44, are also detected. The m/z ratios of 15 and 44 can therefore not be unambiguously assigned to CH_4 or CO_2, since the precursor and the reaction products are present in the deposition chamber at the same time. This can be seen during the precursor step in Figure 2. The measured ion currents at 100°C (dark blue lines) for both m/z ratios can be seen to increase during the precursor pulse (t = 2–7 s). This increase can be fully ascribed to fragments from the precursor. This was confirmed by measuring *precursor only* cycles (not shown): by repeatedly dosing only precursor into the deposition chamber (without subsequent O_2 pulse) the entire surface was saturated preventing any surface reaction products from being formed. The QMS signals measured during a precursor pulse under these saturated conditions therefore only had a precursor component. This precursor signal was then used as a reference for the full cycles, confirming that virtually no reaction products were formed at 100°C. Similarly, *oxygen only* cycles showed that the increase of both signals at 100°C during the O_2 pulse (t = 14–24 s) is also not caused by reaction products. Under the applied conditions the QMS

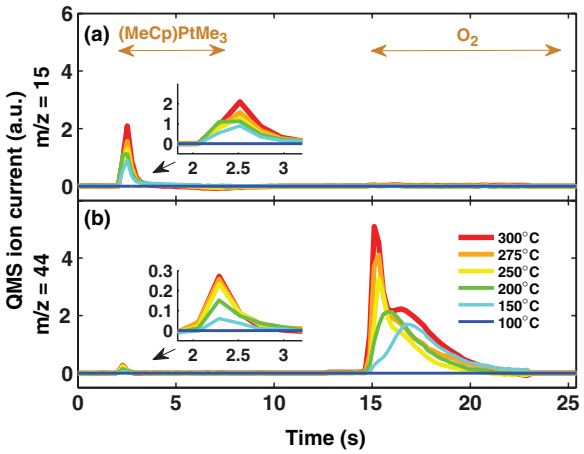

Figure 3. (Color online) Baseline corrected QMS signal as deduced from Figure 2. Data are given for (a) $m/z = 15$ (CH_3^+ from CH_4 and $(MeCp)PtMe_3$) and (b) $m/z = 44$ (CO_2^+ from CO_2). The insets show the signal for CH_4 and CO_2 during the precursor pulse in more detail. The areas under the measured signals represent the amount of reaction products produced at a given temperature.

signal was found to depend on the *total* pressure in the deposition chamber rather than just the partial pressure of O_2. This is referred to here as the pressure artifact. During the O_2 pulse, the pressure inside the deposition chamber and as a result in the QMS detector increases over several orders of magnitude. For such high pressure variations, the QMS signals were found to show a dependence on the total pressure and not merely the partial pressure of a certain species. Peak pressures in the QMS detector of the order of $5 \cdot 10^{-6}$ mbar were detected, which might result in space charge effects in the ionizer and ion-neutral scattering interactions in the mass filter. This could cause deviations from linearity of the detected signal which is known to occur when the pressure inside the ionizer exceeds $\sim 10^{-5}$ mbar.[20] However, both this pressure artifact and the m/z overlap could be corrected for. The *precursor only* and *oxygen only* cycles confirmed that no significant amount of reaction products is formed during deposition at 100°C. While this is different for higher temperatures it shows that the reactor walls, kept at 80°C, will not contribute any significant amount of reaction products, i.e. virtually all reaction products are formed at the substrate stage. Furthermore, this offers the opportunity to use the measurements at 100°C as a reference for the measurements at higher temperatures since the precursor dose and O_2 pressure can be assumed constant over the studied temperature range. By subtracting this reference signal at 100°C from the other measured ion currents, both the precursor m/z overlap effect and the pressure artifact are ipso facto corrected. The result of this correction is plotted in Figure 3, which shows only the net reaction products as will be discussed in the next section.

Results

In Figure 3, the corrected QMS signals for the Pt ALD process can be seen, showing the net production of CH_4 ($m/z = 15$) and CO_2 ($m/z = 44$). Since the signals at 100°C were used as a reference, they are zero during the entire cycle by definition. Peaks in the signals can be seen however at the beginning of the precursor pulse for temperatures of 150°C and above. This indicates that ligand oxidation (leading to CO_2) and other surface reactions (leading to CH_4) can occur at these temperatures. The fact that production of CH_4 and CO_2 only occurs within the first second of the precursor pulse shows that the process reaches saturation after one second of precursor dosing, which was also observed by Kessels et al.[12] For higher temperatures, the amount of reaction products that is formed increases. In the insets of Figure 3, the production of CO_2 is shown to precede the production of CH_4; the signals for CO_2 production start rising and also reach peak value approximately 0.2 s before the signals for CH_4. Figure 3 also shows that during the O_2 pulse, only CO_2 is produced and no CH_4, as was also reported in previous studies.[11–13] Since the QMS signals in Figure 3 have been baseline corrected and show the net production, the area under curve (AUC) is a direct measure for the amount of reaction products that is produced. This was used to quantify the carbon containing reaction products, by assuming that all 9 C-atoms of the precursor molecule are converted into volatile reaction products which are either CH_4 or CO_2. By balancing the AUC of the QMS signals for $m/z = 15$ and 44 for both the precursor and O_2 step at 300°C, the relative amounts of CH_4 and CO_2 could be determined. Firstly however, the AUC values of both species were corrected for partial ionization cross-sections. The total ionization cross-section for CO_2 at 70 eV is $3.56 \cdot 10^{-16}$ cm^2, while CO_2^+ has a partial ionization cross-section of $2.13 \cdot 10^{-16}$cm^2.[21] For CH_4 the total cross-section at 70 eV is $3.54 \cdot 10^{-16}$ cm^2, with a partial cross-section of $1.35 \cdot 10^{-16}$ cm^2 for the production of CH_3^+.[22] Based on measurements at 300°C it was determined that approximately 20% of the carbon is released during the $(MeCp)PtMe_3$ pulse: ~18% as CH_4, and ~2% as CO_2. The remaining 80% are combusted during the O_2 pulse and are converted into CO_2, which agrees nicely with previous results reported by Christensen et al., and Kessels et al.[12,13]

Temperature dependence.— The time-resolved QMS signals in Figure 3 show that during the O_2 pulse the rate of combustion of the hydrocarbon precursor ligands on the Pt surface increases with temperature. At 150°C, CO_2 production reaches peak value approximately 2 seconds after the onset of the O_2 pulse, while at 300°C the peak in production is reached almost instantaneously. Based on the combustion rates during the O_2 pulse, 3 temperature regions can be distinguished:

(i) **T < 100°C:** virtually no combustion occurs.
(ii) **100 < T < 250°C:** combustion occurs at a relatively slow rate, and complete combustion requires several seconds of O_2 dosing.
(iii) **T > 250°C:** combustion occurs almost instantaneously; the bulk of the carbon atoms combusts within the first second of the O_2 pulse.

These temperature regions will be discussed in more detail later on in this section, although it should be noted here that the transitions between these regions are not considered to be sharply defined. Remarkably, at 300°C two distinct peaks can be distinguished: one large peak at the onset of O_2 dosing, and a shoulder that reaches its maximum approximately 2 seconds later. The combustion rate that is displayed by the shoulder is very similar to that of the reaction occurring at approximately 150°C. This suggests that at 300°C set-point temperature, combustion occurs at 2 different reactor zones, each with their own temperature. We therefore attribute the shoulder to reactions on parasitically heated reactor parts near the substrate stage (e.g. the parts holding the stage), that reach elevated temperatures due to heat transfer from the stage. At a heating stage temperature of 300°C these parts might reach temperatures were oxidation proceeds at a slower rate. This effect of parasitic heating also occurs at 250 and 275°C albeit to a much lesser extent. Although this is considered a likely explanation, other explanations (e.g. two distinct and separate reaction pathways leading to CO_2 production) cannot be ruled out at present.

The temperature dependence of the QMS data shows a strong correlation with that of the growth per cycle (GPC) data shown in Figure 1. This graph shows the GPC as a function of deposition temperature for the thermal ALD of Pt as measured with SE. As can be seen, no growth occurs for temperatures below ~100°C, while the GPC appears to saturate as a function of temperature starting at ~250°C, which agrees with the results from Knoops et al.[15] Parallel to the combustion rate, 3 temperature regions can therefore also be distinguished for the GPC:

(i) **T < 100°C:** lack of growth, which coincides with lack of combustion.

(iii) **100 < T < 250°C:** limited growth, which is accompanied by combustion at a reduced rate.
(iii) **T>250°C:** normal growth as well as instantaneous combustion.

The strong correlation between ligand oxidation rate and GPC suggests that the rate of combustion of the ligands during the O_2 step is an important parameter in determining the temperature dependence of Pt ALD growth.

Reactions at 100°C.— To learn more about possible surface reactions at lower temperatures, the process at 100°C was studied in more detail. Although no reactions take place under steady state ALD conditions at 100°C, it is known that plasma assisted ALD of Pt at this temperature is possible.[15] The highly reactive atomic oxygen generated in the plasma ensures complete hydrocarbon removal at the end of every cycle. Therefore, an experiment was devised where standard thermal ALD cycles were preceded by an O_2 plasma treatment. By starting on a plasma-treated surface, surface reactions are expected to occur at least for the first precursor pulse at 100°C. By monitoring the following subsequent cycles individually, valuable information about the process was obtained. Because a plasma was used, reactions could also take place at the reactor walls during this experiment. Therefore, the walls were also heated to 100°C (instead of 80°C), turning the entire deposition chamber into one large reactive surface with one single temperature. Furthermore, for these experiments the reactor walls were completely coated with Pt, to ensure a homogeneous reactive surface composition, and the precursor pulse was increased to 8 seconds to ensure saturation for this larger surface area. The QMS signals of the cycles are shown in Figure 4, and the corresponding AUC values as a function of cycle number (indicating a measure for the amount of reaction products produced) are shown in Figure 5. The graphs in Figure 4 show the as-measured QMS ion currents, i.e. no corrections with respect to a reference have been applied. As a result both the precursor and the pressure artifact are visible. However, cycle 32 can be regarded as a reference because hardly any reaction products are formed anymore during that cycle. This can be inferred from the fact that after cycle 25 the AUC values remained relatively constant and no growth occurred. This can be seen more clearly in Figure 5, where AUC values flatten out beyond cycle 25. The baseline level (indicating a lack of reaction products) that is reached after cycle 25 is represented by the black dotted lines which serve as a guide to the eye.

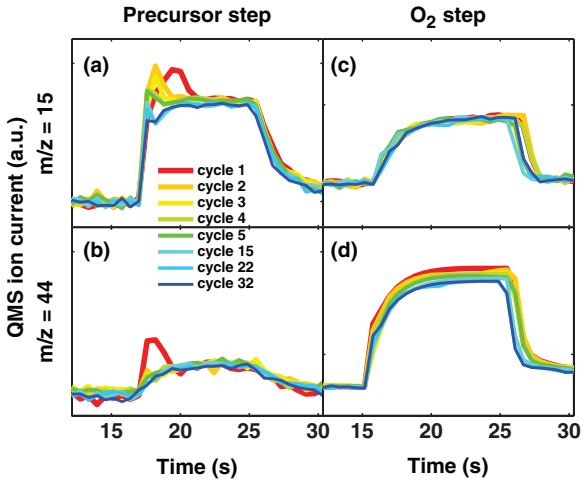

Figure 4. (Color online) The measured QMS signal for (a) $m/z = 15$ and (b) $m/z = 44$ during the precursor pulse, and (c) $m/z = 15$ and (d) $m/z = 44$ during the O_2 pulse; for 32 consecutive ALD cycles, all measured at 100°C. The ALD recipe for all cycles was similar to that of the measurement in Figure 2 (8 s (MeCp)$PtMe_3$, 10 s O_2). However, prior to the first cycle, the entire reactive Pt surface was treated with an O_2 plasma. Since virtually no reaction products are produced during cycle 32, this can be regarded as the baseline level.

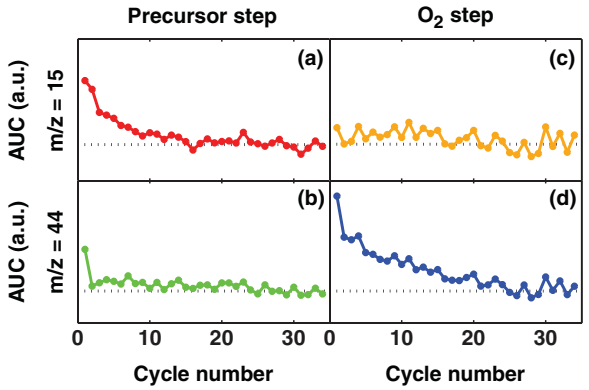

Figure 5. (a-d) The area under curve (AUC) of the measurements shown in Figure 4, representing the amount of reaction products as a function of cycle number. Prior to the first cycle the Pt surface was treated with an O_2 plasma. Baseline values that are reached after cycle 25 are indicated by the black dotted lines which serve as a guide to the eye.

The signals in Figure 4 will now be considered cycle-by-cycle, starting at cycle 1, which was the first standard ALD cycle following the plasma treatment. Clearly, reaction products are indeed formed during this cycle. The production of CH_4 and CO_2 is evident from the peaks in the signals that are observed at the beginning of the precursor pulse in Figures 4a and 4b. The peaks in Figures 4a and 4b are broader, i.e. the signals increase over a longer period of time compared to the signals during the peaks in Figure 2. This indicates that reactions proceed for a longer period of time. The longer reaction times are most likely due to the fact that the precursor requires more time to saturate the larger reactive surface. It is also possible however that the increased reaction time is caused by slower reaction kinetics due to the lower temperature. Because the reactions are stretched out over a longer period of time, it becomes even clearer that the production of CO_2 precedes the production of CH_4. Furthermore, during the precursor step of the next cycle (cycle 2), the production of CO_2 has disappeared almost completely, while the production of CH_4 still persists. Because the reaction pathway leading to CH_4 is now unhindered by competing combustion reactions, this pathway becomes more dominant, and CH_4 is produced at the very onset of precursor dosing. This clearly demonstrates that the production of CH_4 is a separate process that does not necessarily depend upon the production of CO_2, at least at a temperature of 100°C. During the following cycles, the amount of CH_4 production gradually decreases until it reaches baseline values around cycle 25. Considering the O_2 pulse, see Figures 4c and 4d, no production of CH_4 was detected during any cycle as expected. Some CO_2 is produced during the first cycles (compared to reference cycle 32) although there is no clear peak as was seen in Figure 2. This indicates that although there is some carbon combustion during the first cycles after the plasma treatment, combustion is far less effective than at 300°C. During the following cycles the amount of CO_2 that is produced continuously decreases up to approximately cycle 25. After cycle 25, the CO_2 signal remains relatively constant indicating combustion has ceased. The decrease in the amount of reaction products can also be seen in the AUC values in Figure 5. The amount of CH_4 during the precursor step slowly decreases over several cycles, while the production of CO_2 drops to baseline immediately after cycle 1. This shows nicely that the production of CH_4 persists even after the production of CO_2 has ceased. During the O_2 step, the amount of combustion products continuously decreases, while no production of CH_4 can be seen. During this experiment, SE data was also recorded which showed an increase of apparent thickness of 0.1 nm over cycle 1 (GPC for plasma assisted ALD of Pt at 100°C is normally 0.045 nm), while during the following cycles virtually no growth was detected. The relatively large increase during the first cycle indicates that precursor molecules did adsorb during the precursor pulse, but that their ligands were not completely combusted during the O_2 pulse.

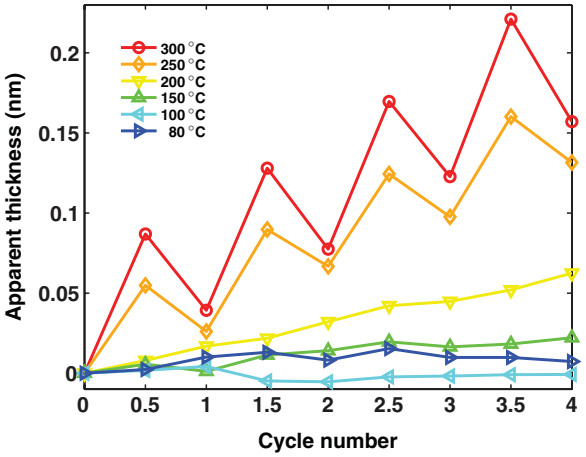

Figure 6. The apparent thickness of the films obtained from SE, performed every half-cycle for ALD at different substrate temperatures different temperatures. The half-integer and full-integer data points represent SE measurements after the precursor and O_2 pulse, respectively.

Summarizing these results, the study of the thermal process following plasma treatment at 100°C indicates that no growth occurs at this temperature due to the lack of ligand combustion. When chemisorbed oxygen is available however (due to e.g. a plasma treatment), precursor molecules can adsorb with their ligands reacting into CO_2 and CH_4. In the absence of chemisorbed oxygen, only CH_4 can be produced until reactions become prevented by some form of surface blocking.

Spectroscopic ellipsometry.— Whereas growth below 100°C is completely inhibited for the thermal process, between 100 and 250°C growth does occur albeit at lower growth rates, as was depicted in Figure 1. The temperature regime in which this occurs coincides with the production of CO_2 at reduced reaction rates during the O_2 pulse (see Figure 3). To examine the growth behavior more closely, additional SE measurements were performed at temperatures between 80 and 300°C. The data is shown for 4 cycles in Figure 6. The thickness was measured after every half-cycle, i.e. after every precursor and after every O_2 step. Once again, three distinct temperature regions become apparent. Above 250°C, a sawtooth-shaped curve is obtained. Between 100 and 250°C this sawtooth shape can no longer be seen, although there is still some growth. At temperatures of 100°C and below, the apparent thickness remains virtually constant, indicating very little or no growth. The characteristic sawtooth-shaped curve that was observed for temperatures above 250°C, can be explained by considering the apparent thickness of the surface.[18] After the precursor pulse, the thickness of the layer will have increased with the newly deposited Pt as well as the adsorbed precursor ligands which have not yet been eliminated. The SE model that was used in these experiments assumes that the dielectric properties of the layer are constant. The thickness of the layer was the only parameter that was varied to fit the data. Therefore, the uncombusted ligands could cause a relatively large increase in the apparent thickness of the layer, greater than the GPC. During the subsequent O_2 pulse the excess ligands are combusted, causing a (smaller) decrease in apparent thickness. The difference between the increase in apparent thickness during the precursor step, and the decrease in apparent thickness during the O_2 step, yields the GPC.

By combining the insights gained from the experiments described above, a more comprehensive model of the temperature dependence of the reaction mechanism can be obtained as well as a better understanding of individual reaction paths, as will be discussed in the next section.

Discussion

The implications of the results shown in the previous section for our understanding of the reaction mechanism of Pt ALD will be discussed here.

Temperature dependence.— (i) **T < 100°C** Starting at lower temperatures, it is clear from Figure 1 that no growth occurs at ∼100°C. Figure 3 shows furthermore, that no reaction products are formed at this temperature. A possible explanation for the lack of growth and reaction products could be poor precursor adsorption at lower temperatures. However, adsorption of the precursor has been reported even at room temperature.[23] Furthermore, it is known that plasma assisted ALD of Pt is possible at 100°C, and in the plasma treatment experiment shown in Figure 4 reaction products were observed during the 1st cycle. This confirms that the precursor can adsorb at 100°C. Another possible explanation for growth inhibition would be the lack of chemisorbed surface oxygen at the onset of the precursor pulse. However, according to Getman et al. the oxygen surface coverage of a Pt(111) surface in equilibrium with O_2 gas, should not depend on temperature in the ALD range.[24] This coverage was found to be 0.25 monolayers (ML) on Pt(111) for the temperatures and pressures used in the Pt ALD process.[25] The presence of surface oxygen at 100°C is also indicated by the fact that CO_2 was detected during the first cycle after the plasma treatment (see Figure 4b). The amount of chemisorbed oxygen that can cover a clean Pt surface at a temperature of 100°C should therefore not be the limiting factor inhibiting growth either. One remaining possible cause is the incomplete combustion of the precursor ligands during the O_2 pulse. The data in Figure 1 and Figure 3 show a clear correlation between a reduced GPC and the reduced level of combustion during the O_2 pulse at lower temperatures. Reduced combustion was also indicated by the relatively small amount of CO_2 that was detected during the O_2 pulse for the cycles following the plasma treatment (Figure 4d). Furthermore, the experiments involving a plasma treatment also showed that beyond the first cycle, no CO_2 was produced during the precursor pulse, even though the production of CH_4 continued (Figure 4a, 4b). This suggests that under these conditions no chemisorbed oxygen is available at the beginning of the precursor pulse. In order to explain the lack of chemisorbed oxygen, the state of the platinum surface after the precursor pulse should be considered.

The $(MeCp)PtMe_3$ precursor contains both methyl (Me) and methylcyclopentadienyl (MeCp) ligands. Due to the catalytic nature of Pt however, it is likely that some of the ligands on the surface will become fragmented upon precursor adsorption.[17] For conceptual clarity however, the initial species on the surface after precursor adsorption are assumed here to be either Me or MeCp. The fact that the MeCp ligand was not detected as a volatile reaction product in this work or in the QMS study of Christensen et al. indicates that this ligand remains at the surface.[13] In our previous work on the Pt ALD mechanism, a compelling case was made for the use of results from surface science literature.[17] The behavior of hydrocarbon species on Pt surfaces was discussed extensively, and the relevant results will be discussed here. The surface chemistry of Me groups on a Pt (111) surface can be described as a competition between hydrogenation producing CH_4, and dehydrogenation reactions forming hydrocarbon species that have a relatively high C/H ratio.[26,27] The desorption of methane takes place for temperatures of −73°C and higher.[27] Concerning the behavior of MeCp on a Pt surface, results reported for other cyclic hydrocarbon species can be useful since different cyclic hydrocarbon species are reported to behave similarly on Pt.[28] Marsh et al. describe temperature programmed desorption (TPD) measurements of a benzene covered Pt(111) surface.[29] In their experiment, the substrate temperature was gradually raised while the substrate was exposed to O_2. They found that below a temperature of 107°C the pre-adsorption of benzene on the Pt (111) inhibits the adsorption of oxygen as a result of which hydrocarbon oxidation is inhibited. Given the agreement between results from Marsh et al. and those reported here, it is plausible that a similar inhibition of ligand combustion occurs during the Pt ALD process at temperatures of ∼100°C. At these temperatures, both the MeCp ligands and the carbon-rich products of MeCp / Me dehydrogenation could form a carbonaceous layer that blocks surface sites required for O_2 dissociation, thereby preventing combustion. This is corroborated by the fact that in Figure 4b no CO_2 is produced during the precursor pulse beyond cycle 1. The relatively

small and decreasing amount of combustion products during the O_2 pulse (Figure 4d) also indicates a gradual "poisoning" of the Pt surface by carbonaceous surface species. Similarly, the surface species could inhibit further hydrogenation of Me ligands preventing CH_4 production. Evidence of this inhibition can be seen in Figure 4a, where the production of CH_4 gradually extinguishes in the subsequent cycles. The presence of the unreactive hydrocarbon species might thereby inhibit growth by hindering hydrogenation and by blocking oxygen chemisorption. This would also explain why plasma-assisted deposition is possible at low temperatures; the oxygen radicals that are generated in the plasma do not need to be dissociated at the Pt surface and can react directly with the hydrocarbon fragments on the surface.

(ii) **100<T<250°C** The Pt ALD process between 100 and 250°C is characterized by an increase in the GPC as well as an increase in the amount of CH_4 and CO_2 produced in the precursor pulse. Furthermore, the reaction rate for combustion during the O_2 pulse increases as a function of temperature, although combustion is not yet instantaneous (see Figure 3). Apparently, due to the increase in substrate temperature, a larger amount of precursor molecules can absorb due to increased ligand combustion during the O_2 pulse. An explanation for this increase in combustion can be found by once again considering the Me/MeCp-covered platinum surface. In their TPD experiments of a benzene covered Pt surface exposed to O_2, Marsh et al. reported the production of CO_2 and H_2O for temperatures between 107–347°C.[29] They ascribed the oxidation of benzene to a reaction between benzene derived intermediates and atomic oxygen at the surface. The temperature range in which Marsh et al. observed the production of CO_2 and H_2O coincide remarkably with the onset of the formation of combustion products presented in this work. This indicates that the MeCp group starts to react with oxygen above ~100°C. Furthermore, it is likely that MeCp can start to undergo dehydrogenation in the temperature region between ~100 and ~250°C: Cp is reported to start to dehydrogenate on a Pt surface for temperatures above 223°C, while benzene dehydrogenates above 177°C.[30–32] Clearly, in the temperature range between 100 and 250°C MeCp becomes more reactive with the surface. Some of the MeCp groups could form intermediates or start to break into smaller hydrocarbon groups by dehydrogenation. Furthermore, the products of dehydrogenation of the Me and MeCp species are likely to change as a function of temperature. The increased reactivity of the MeCp with the surface and the possible change in dehydrogenation reaction products can lead to a change in the composition and thickness of the carbonaceous layer that is formed during the precursor pulse. This would free up more sites for oxygen chemisorption which will lead to increased combustion. A final possible cause for the increased reaction product formation and growth is the increased combustion rate at higher temperatures which was observed in Figure 3.

While it is difficult to give a precise description of all the surface species and surface reactions, it does seem likely that an increase in surface temperature has the following two effects: a change in composition of the surface species allowing more oxygen chemisorption, and enhanced combustion reactions. A combination of these effects could lead to increased ligand combustion, subsequent increased precursor adsorption, and therefore, increased growth per cycle. This explanation is in line with the SE measurements shown in Figure 6. When SE measurements are performed every half-cycle during normal Pt ALD growth (i.e. at 300°C), the apparent thickness of the film can increase upon precursor adsorption, due to the bulky ligands that remain at the surface. After the subsequent O_2 pulse these ligands are combusted, which could cause a relative decrease in apparent thickness. Between 100 and 250°C however, the amount of precursor molecules that adsorb is too small to cause a noticeable change in apparent thickness, since the surface is already covered with a carbonaceous layer at the beginning of the precursor pulse. Similarly, the small amount of ligands that is combusted during the O_2 pulse causes only a negligible change in apparent thickness. The growth caused by the small amount of precursor molecules that adsorbs can only be detected when measured over several cycles.

(iii) **T > 250°C.** The temperature region between 250 and 300°C is characterized by a growth per cycle that seems to flatten for higher temperatures (Figure 1), sawtooth shaped SE half-cycle curves (Figure 6), and instantaneous combustion during the O_2 pulse (Figure 2). At these temperatures the hydrocarbon species at the Pt surface are fragmented to such an extent that oxygen can chemisorb unhindered and react immediately with these species until virtually all surface carbon is removed.

Reactions at 300°C.— The study of the temperature dependence of the reaction mechanism presented in this work also provides insight into Pt ALD at 300°C, which is the typically employed deposition temperature for this process. The involvement of dehydrogenation reactions has been suggested by Mackus et al. to explain the formation of CH_4 during the precursor pulse.[17] They describe the surface reactions as a competition between these dehydrogenation reactions and combustion reactions, where the latter take precedence provided a sufficient supply of oxygen is available. When most of the oxygen has been consumed, the production of CO_2 will diminish and be replaced by CH_4 formation. This explains why CH_4 is produced during the precursor pulse only. The proposed competition between combustion and hydrogenation reactions for the available surface carbon is supported by the time-resolved QMS data in Figures 3 and 4. In both figures the production of CO_2 is shown to precede CH_4 formation, although the distinction is much clearer for the first cycle in Figure 4. The peak in CH_4 formation occurs approximately 2 seconds after the peak in CO_2 production. During the following cycles, the absence of CO_2 production causes CH_4 to be produced earlier after the start of the precursor pulse and at an increased rate. This clearly points to a competition between these two reactions and supports the occurrence of dehydrogenation reactions. The fact that the data in Figure 4 was obtained at 100°C should not be of major influence given that the reaction kinetics during the precursor pulse do not seem to depend greatly on temperature as can be seen in Figure 3. Further indications that dehydrogenation reactions play a role in the reaction mechanism of Pt ALD can be found by evaluating the reaction mechanism (Equation 1 and 2). In this reaction mechanism equation, which was based on an FTIR study, the ratio of CH_4 / CO_2 production during the precursor pulse was found to be 1:1.[12] One CH_3 ligand is combusted by 2 O atoms, releasing 3 H atoms. These 3 H atoms are sufficient to produce 1 H_2O molecule and hydrogenate 1 Me ligand from another precursor molecule to produce CH_4. The combustion of 1 Me ligand therefore provides the hydrogen for the production of 1 CH_4 molecule. In this work however, as well as in the study by Christensen, the CH_4 / CO_2 ratio was found to be 6 to 9 times higher. Assuming the ratio is larger than 1, this excess CH_4 production during the precursor pulse requires an additional source of H atoms. Since hydroxyl (OH) groups or H_2O are not expected to be stable on the Pt surface, the only available source for this H is the precursor ligands themselves.[33] Since the combustion of ligands is insufficient to supply the hydrogen (CH_4 / CO_2 >1), the likely alternative would be the dehydrogenation of other Me or MeCp ligands. Therefore, the relatively high amount of CH_4 production during the precursor pulse implies that dehydrogenation reactions take place. Since the CH_4 / CO_2 ratio is relevant for this matter, the different values found in the mentioned studies will be discussed briefly. A possible explanation for the differences in the ratio of the reaction products could be found in the measurement techniques that were used, and differences in process parameters (see Table I). During both QMS studies, the reaction products were measured in real-time, while during the FTIR study a single measurement lasted up to 5 minutes. Furthermore, while performing the FTIR measurements, all reaction products were confined to the deposition chamber, and it cannot be excluded that this leads to additional or different reactions. Despite the differences in CH_4 / CO_2 ratio, the overall reaction mechanism is expected to be similar, since all 3 studies show that the majority of the carbon is combusted during the O_2 pulse.

Table I: Summary of the results of several studies with respect to the amount of reaction products that are produced during Pt ALD. Relevant process parameters are also listed.

		Precursor step		O_2 step		O_2	Substrate	Wall
Reference	Technique	CH_4	CO_2	CH_4	CO_2	Pressure	Temperature	Temperature
12	FTIR	6.5%	6.5%	0	87%	1 mbar	300°C	80°C
13	QMS	18%	3%	0	79%	1.3 mbar	300°C	300°C
This work	QMS	18%	2%	0	80%	0.08 mbar	300°C	80°C

Conclusions

Time-resolved QMS and in-situ SE results in combination with insights from surface science studies were used to investigate the reaction mechanism of Pt ALD. An investigation of the temperature dependence showed that the process can roughly be divided into 3 temperature regions. At and below 100°C, growth is inhibited and virtually no reaction products are formed. Between 100°C and 250°C, the GPC, the amount of reaction products, and the rate of combustion increase as a function of temperature. Above 250°C, the GPC is relatively constant while combustion occurs instantaneously and is complete. Monitoring the process after a plasma treatment with QMS and in-situ SE showed that the lack of growth at low temperatures cannot be ascribed to poor precursor adsorption or reduced oxygen chemisorption, but is due to lack of ligand combustion. An explanation for the temperature dependence of the reaction mechanism was found by considering the possible behavior of MeCp and Me on the surface. Below 100°C, the MeCp ligand remains uncombusted and can form a carbonaceous layer together with the carbon-rich products of MeCp / Me dehydrogenation. This carbonaceous layer might block sites required for oxygen dissociation. Above 100°C, MeCp may start to dehydrogenate (allowing for CH_4 production) and the increased temperature may change the composition and thickness of the carbonaceous layer. This would allow oxygen to dissociate leading to CO_2 production. Furthermore, ligand combustion may proceed at faster rates for elevated temperatures. Above 250°C, the surface groups have been fragmented by dehydrogenation or other reactions to such an extent that oxygen can dissociate and chemisorb on the surface unhindered, and combustion occurs instantaneously.

Quantification of the QMS data at 300°C indicated that approximately 20% of all precursor carbon atoms react during the precursor pulse: ∼18% as CH_4, and ∼2% as CO_2. The remaining 80% of the precursor carbon is combusted during the O_2 pulse. The fact that more CH_4 than CO_2 is produced during the precursor pulse suggests that the dehydrogenation of the Me and MeCp ligands supplies the required H for hydrogenation of Me to form CH_4. The time-resolved QMS data indicated that combustion and hydrogenation reactions (producing CO_2 and CH_4, respectively) compete for the available surface carbon and that combustion is the dominant reaction provided a sufficient supply of oxygen is available.

The reaction mechanism of Pt ALD has been discussed on the basis of the behavior of both Me and MeCp on the Pt surface. As mentioned previously, it should be noted that the actual state and composition of the hydrocarbon species on the Pt surface may change due to catalytic activity of the surface. Since this catalytic behavior is also displayed by other Pt group metals, the conclusions that are drawn here could possibly be generalized to other precursors (with other hydrocarbon ligands) and even to other noble metal ALD processes.[17] For the ALD of Ru, Os, Rh, Ir and Pt with O_2 as a reactant, a substrate temperature of at least 200°C is required to obtain deposition of high-quality films.[34–38] Furthermore, the nature of the precursor ligands does not seem to have a large influence on the lower limit of the temperature window. For Ir ALD for example, high-quality films can be deposited for substrate temperatures above ∼220°C, regardless of whether Ir(EtCp)(COD), Ir(acac)$_3$, or (MeCp)Ir(CHD) precursor is used. All Pt-group metals show a similar ability to break C–H bonds of adsorbed species, independent of specific precursor ligands. Therefore, a reaction mechanism and temperature dependence similar to that of Pt ALD may also apply to other noble metal ALD processes.

Acknowledgments

This research has been supported financially by IMEC-NL, the Netherlands. The research of one of the authors (W.M.M. Kessels) is supported by the Netherlands Organization for Scientific Research (NWO) and the Technology Foundation STW through the VICI program on "Nanomanufacturing". Special thanks to Janneke Zeebregts, Ries van de Sande, and Joris Meulendijks for their technical support.

References

1. K. J. Albert, N. S. Lewis, C. L. Schauer, G. A. Sotzing, S. E. Stitzel, T. P. Vaid, and D. R. Walt, *Chemical Reviews*, **100**, 2595 (2000).
2. H. Seo, T. Endoh, H. Fukuda, and S. Nomura, *Electronics Letters*, **33**, 535 (1997).
3. K. Tsukada, T. Kiwa, T. Yamaguchi, S. Migitaka, Y. Goto, and K. Yokosawa, *Sensors and Actuators B-Chemical*, **114**, 158 (2006).
4. M. S. H. Abadi, M. Gholizadeh, and A. Salehi, *Sensors and Actuators B-Chemical*, **141**, 1 (2009).
5. M. Zhang, Z. Yuan, J. Song, and C. Zheng, *Sensors and Actuators B: Chemical*, **148**, 87 (2010).
6. X. Y. Xue, Z. H. Chen, C. H. Ma, L. L. Xing, Y. J. Chen, Y. G. Wang, and T. H. Wang, *Journal of Physical Chemistry C*, **114**, 3968 (2010).
7. D. Haridas, K. Sreenivas, and V. Gupta, *Sensors and Actuators B: Chemical*, **133**, 270 (2008).
8. D. J. Comstock, S. T. Christensen, J. W. Elam, M. J. Pellin, and M. C. Hersam, *Advanced Functional Materials*, **20**, 3099 (2010).
9. D. Haridas, A. Chowdhuri, K. Sreenivas, and V. Gupta, *Sensors and Actuators B-Chemical*, **153**, 89 (2011).
10. T. Aaltonen, M. Ritala, T. Sajavaara, J. Keinonen, and M. Leskelä, *Chem. Mater.*, **15**, 1924 (2003).
11. T. Aaltonen, A. Rahtu, M. Ritala, and M. Leskelä, *Electrochem. Solid-State Lett.*, **6**, C130 (2003).
12. W. M. M. Kessels, H. C. M. Knoops, S. A. F. Dielissen, A. J. M. Mackus, and M. C. M. van de Sanden, *Appl. Phys. Lett.*, **95**, 013114 (2009).
13. S. T. Christensen and J. W. Elam, *Chem. Mater.*, **22**, 2517 (2010).
14. W. Setthapun, W. D. Williams, S. M. Kim, H. Feng, J. W. Elam, F. A. Rabuffetti, K. R. Poeppelmeier, P. C. Stair, E. A. Stach, F. H. Ribeiro, J. T. Miller, and C. L. Marshall, *J. Phys. Chem. C*, **114**, 9758 (2010).
15. H. C. M. Knoops, A. J. M. Mackus, M. E. Donders, M. C. M. van de Sanden, P. H. L. Notten, and W. M. M. Kessels, *Electrochem. Solid-State Lett.*, **12**, G34 (2009).
16. S. D. Elliott, *Langmuir*, **26**, 9179 (2010).
17. A. J. M. Mackus, N. Leick, L. Baker, and W. M. M. Kessels, *Chem. Mater.*, **24**, 1752 (2012).
18. E. Langereis, S. B. S. Heil, H. C. M. Knoops, W. Keuning, M. C. M. van de Sanden, and W. M. M. Kessels, *J. Phys. D: Appl. Phys.*, **42**, 073001 (2009).
19. H. C. M. Knoops, E. Langereis, M. C. M. van de Sanden, and W. M. M. Kessels, *Journal of Vacuum Science & Technology A*, **30**, 01A101-1/10 (2012).
20. Stanford research systems user manual QMS 100 series gas analyzer 2000.
21. Y. Itikawa, *J. Phys. Chem. Ref. Data*, **31**, 749 (2002).
22. H. C. Straub, D. Lin, B. G. Lindsay, K. A. Smith, and R. F. Stebbings, *J. Chem. Phys.*, **106**, 4430 (1997).
23. J. J. L. Mulders, L. M. Belova, and A. Riazanova, *Nanotechnology*, **22**, 055302 (2011).
24. R. B. Getman, Y. Xu, and W. F. Schneider, *J. Phys. Chem. C*, **112**, 9559 (2008).
25. G. N. Derry and P. N. Ross, *Surf. Sci.*, **140**, 165 (1984).
26. F. Zaera, *Surf. Sci.*, **262**, 335 (1992).
27. F. Zaera and H. Hoffmann, *J. Phys. Chem.*, **95**, 6297 (1991).
28. W. L. Manner, G. S. Girolami, and R. G. Nuzzo, *Langmuir*, **14**, 1716 (1998).
29. A. L. Marsh, D. J. Burnett, D. A. Fischer, and J. L. Gland, *Journal of Physical Chemistry B*, **107**, 12472 (2003).
30. N. R. Avery, *J. Electron Spectrosc. Relat. Phenom.*, **39**, 1 (1986).
31. N. R. Avery, *Surf. Sci.*, **146**, 363 (1984).
32. C. T. Campbell, J. M. Campbell, P. J. Dalton, F. C. Henn, J. A. Rodriguez, and S. G. Seimanides, *J. Phys. Chem.*, **93**, 806 (1989).

33. A. Shavorskiy, T. Eralp, M. J. Gladys, and G. Held, *J. Phys. Chem. C*, **113**, 21755 (2009).
34. T. Aaltonen, M. Ritala, and M. Leskelä, *Electrochem. Solid-State Lett.*, **8**, C99 (2005).
35. J. Hamalainen, T. Sajavaara, E. Puukilainen, M. Ritala, and M. Leskela, *Chemistry of Materials*, ASAP (2011).
36. T. Aaltonen, M. Ritala, V. Sammelselg, and M. Leskela, *J. Electrochem. Soc.*, **151**, G489 (2004).
37. T. Aaltonen, M. Ritala, Y. L. Tung, Y. Chi, K. Arstila, K. Meinander, and M. Leskelä, *J. Mater. Res.*, **19**, 3353 (2004).
38. T. Aaltonen, P. Alen, M. Ritala, and M. Leskela, *Chem. Vap. Deposition*, **9**, 45 (2003).